

Probing the Majorana bound states in a hybrid nanowire double-quantum-dot system by scanning tunneling microscopy

Jia Liu(刘佳), Ke-Man Li(李科曼), Feng Chi(迟锋), Zhen-Guo Fu(付振国), Yue-Fei Hou(侯跃飞), Zhigang Wang(王志刚), Ping Zhang(张平)

Citation: Chin. Phys. B . 2020, 29(7): 077302 . **doi:** 10.1088/1674-1056/ab8889
Journal homepage: http://cpb.iphy.ac.cn; http://iopscience.iop.org/cpb

What follows is a list of articles you may be interested in

Zero-energy modes in serially coupled double quantum dots

Fu-Li Sun(孙复莉), Zhen-Hua Li(李振华), Jian-Hua Wei(魏建华)
Chin. Phys. B . 2020, 29(6): 067302 . **doi:** 10.1088/1674-1056/ab8378

Single-electron transport through single and coupling dopant atoms in silicon junctionless nanowire transistor

Xiao-Di Zhang(张晓迪), Wei-Hua Han(韩伟华), Wen Liu(刘雯), Xiao-Song Zhao(赵晓松), Yang-Yan Guo(郭仰岩), Chong Yang(杨冲), Jun-Dong Chen(陈俊东), Fu-Hua Yang(杨富华)
Chin. Phys. B . 2019, 28(12): 127302 . **doi:** 10.1088/1674-1056/ab527a

Enhanced spin-dependent thermopower in a double-quantum-dot sandwiched between two-dimensional electron gases

Feng Chi(迟锋), Zhen-Guo Fu(付振国), Liming Liu(刘黎明), Ping Zhang(张平)
Chin. Phys. B . 2019, 28(10): 107305 . **doi:** 10.1088/1674-1056/ab3f98

Phase diagram characterized by transmission in a triangular quantum dot

Jin Huang(黄金), Wei-Zhong Wang(王为忠)
Chin. Phys. B . 2018, 27(11): 117303 . **doi:** 10.1088/1674-1056/27/11/117303

Enhanced transient photovoltaic characteristics of core-shell ZnSe/ZnS/L-Cys quantum-dot-sensitized TiO_2 thin-film

Kui-Ying Li(李葵英), Lun Ren(任伦), Tong-De Shen(沈同德)
Chin. Phys. B . 2018, 27(6): 067305 . **doi:** 10.1088/1674-1056/27/6/067305

Probing the Majorana bound states in a hybrid nanowire double-quantum-dot system by scanning tunneling microscopy*

Jia Liu(刘佳)[1], Ke-Man Li(李科曼)[1], Feng Chi(迟锋)[2], Zhen-Guo Fu(付振国)[3,†], Yue-Fei Hou(侯跃飞)[3], Zhigang Wang(王志刚)[3], and Ping Zhang(张平)[3,‡]

[1] *School of Science, Inner Mongolia University of Science and Technology, Baotou* 014010, *China*
[2] *School of Electronic and Information Engineering, Zhongshan Institute, University of Electronic Science and Technology of China, Zhongshan* 528400, *China*
[3] *Institute of Applied Physics and Computational Mathematics, Beijing* 100088, *China*

(Received 8 January 2020; revised manuscript received 7 April 2020; accepted manuscript online 12 April 2020)

We propose an interferometer composing of a scanning tunneling microscope (STM), double quantum dots (DQDs), and a semiconductor nanowire carrying Majorana bound states (MBSs) at its ends induced by the proximity effect of an s-wave superconductor, to probe the existence of the MBSs in the dots. Our results show that when the energy levels of DQDs are aligned to the energy of MBSs, the zero-energy spectral functions of DQDs are always equal to $1/2$, which indicates the formation of the MBSs in the DQDs and is also responsible for the zero-bias conductance peak. Our findings suggest that the spectral functions of the DQDs may be an excellent and convenient quantity for detecting the formation and stability of the spatially separated MBSs in quantum dots.

Keywords: quantum dot, scanning tunneling microscopy, Majorana bound states

PACS: 73.21.La, 68.37.Ef, 05.60.Gg **DOI:** 10.1088/1674-1056/ab8889

1. Introduction

In recent years, Majorana bound states (MBSs), which are fundamentally solid state counterpart of Majorana fermions that are their own antiparticles in high-energy physics, have been extensively studied theoretically and experimentally.[1,2] They are zero-energy quasiparticles realized at the edges or at topological defects of nontrivial superconductors, and are topologically protected.[3–9] The topological protection, which is based on the separation of a pair of MBSs, results in the non-abelian statistics making MBSs ideal building blocks for topological quantum computation free from decoherence.[10,11] With the rapid development of nano-fabrication techniques, topologically protected MBSs are now mainly realized from the spatially separated Andreev bound states (ABSs) in hybrid superconductor-semiconductor nanowires.[12–18]

Since it is easy to control their electronic properties, the quantum dots (QDs),[19–30] quantum rings,[31] as well as Josephson junctions[17,32–34] may be excellent platforms to detect the MBSs in solids. Experimentally, a series of quantum transport measurements for MBSs embedded in a semiconducting nanowire (with proximity-induced superconductivity) coupled to a QD have been performed. As an example, Deng *et al.*[15,16] put forward a spectrometer comprised of a semiconducting nanowire with proximity-induced superconductivity for the degree of Majorana nonlocality in a QD by measuring the zero-bias conductance peak (ZBCP) under various conditions. However, in fact, the ZBCP can also originate from other physical mechanisms, such as the Kondo effect, disorder, and the ABSs in hybrid devices. To clarify the origin of the ZBCP observed in the quantum transport measurements, several theoretical schemes were proposed to analyze the tunneling spectroscopy of a QD which is coupled to both ends of the nanowire hosting the MBSs. For instance, Liu *et al.*[26] theoretically considered the interplay between ABSs and MBSs in disorder-free QD nanowire semiconductor systems with proximity-induced superconductivity. Zhang *et al.* have successfully measured a quantized conductance plateau at $2e^2/h$ in the zero-bias conductance in indium antimonide semiconductor nanowires covered with an aluminium superconducting shell, which supports the existence of Majorana zero-modes therein and may pave a way for the experiments that could lead to topological quantum computing.[28,30] More recently, a definitive detection of the parity anomaly in a topological superconductor ring was also proposed.[31] Furthermore, Floquet MBSs (zero mode and π mode) were theoretically studied in planar Josephson junctions, in which the subharmonic response to the external drive tuned by a top gate was found when both zero and π Majorana modes are present.[34] Additionally, in the latest reports,[35–38] nanosystems consisting of a hybrid superconducting nanowire coupled to a single

*Project supported by the National Natural Science Foundation of China (Grant Nos. 11564029 and 11675023), the Natural Science Foundation of Inner Mongolia, China (Grant No. 2017MS0112), the Science Foundation for Excellent Youth Scholors of Inner Mongolia University of Science and Technology, China (Grant No. 2017YQL06), the Initial Project of UEST of China, Zhongshan Institute (Grant No. 415YKQ02), the Science and Technology Bureau of Zhongshan City, China (Grant Nos. 2017B1116 and 2017B1016), and the Innovation Team of Zhongshan City, China (Grant No. 180809162197886).

†Corresponding author. E-mail: fu_zhenguo@iapcm.ac.cn
‡Corresponding author. E-mail: zhang_ping@iapcm.ac.cn

© 2020 Chinese Physical Society and IOP Publishing Ltd

QD and/or double quantum dots (DQDs) attached to a single normal metallic lead have been theoretically discussed.

Meanwhile, scanning tunneling microscopy (STM)[39–42] measurements of MBSs in condensed matters have also been extensively carried out to study the electronic and spintronic properties of MBSs. Compared to the conventional quantum transport techniques, the STM has its own advantages in probing and even manipulating MBSs, from which the more precise quantum processes and mechanisms become possible to reveal. In particular, due to the nontrivial topological nature of MBSs, *in situ* designing of specific MBS configurations can be harnessed to image extraordinary quantum properties of MBSs. Recently, Sun *et al*. have probed the spin selective Andreev reflection of Majorana zero modes in a topological superconductor of the $Bi_2Te_3/NbSe_2$ heterostructures using a spin-polarized scanning tunneling microscope (STM). The spin dependent tunneling effect observed in their STM experiments provides direct evidence of Majorana zero modes (MZM).[43] More recently, by employing a spin-polarized STM, Jeon *et al*. have also experimentally found that MBSs realized in self-assembled Fe chains on the surface of Pb have a spin polarization that exceeds the value stemming from the magnetism of these chains.[44] By using an STM, a zero-bias peak inside a vortex core induced by MBSs has been observed on the superconducting Dirac surface state of the iron-based superconductor $FeTe_{0.55}Se_{0.45}$.[45–47] Jäck and his collaborators have also performed the STM measurements for probing the MZM in a topologically protected edge of bismuth(111) films.[48] Most recently, Chen *et al.* have reported their STM experimental finding of MZM simultaneously appearing at both ends of a one-dimensional atomic line defect in monolayer iron-based superconductor $FeTe_{0.5}Se_{0.5}$.[49] Additionally, QD molecules have been successfully constructed on a semiconductor surface using atom manipulation by STM.[50] On the theoretical side, the possibility to detect the spatial profile of Majorana fermions by using STM tips that are made of either a normal or a superconducting material have also been investigated, but no quantum dot is taken into account.[51–54]

Motivated by both advanced quantum transport measurements for MBSs through QD coupled with topological superconducting nanowires[15,16] and dramatic STM measurements of MBSs on the surfaces of topological superconductors,[43,44] we would like to theoretically consider a model which is composed of an STM tip and DQDs coupled to the ends of nanowire where MBSs are induced due to the proximity effect of superconductivity, see Fig. 1. Differing from most of the previous quantum transport models reported in literature, in which QD usually couples to double (left and right) leads, in our present model we just consider a single normal metallic lead, i.e., the STM tip. Moreover, we emphasize that in our model, DQDs are taken into account, from which the spectral function of each QD may provide significant information about the effective tunneling (or not) of the MBSs into the QD. By comparing the spectral functions for the cases with and without coupling between the DQD and MBSs, two generic types of signatures of the MBSs presence in QD-1 or QD-2 may be identified.

2. Model and method

As shown in Fig. 1, DQDs are connected to the STM tip with different coupling strengths V_1 and V_2, and to the MBSs, which are denoted by η_1 and η_2, at the two ends of a semiconductor-superconductor nanowire with hybridizations λ_1 and λ_2, respectively. The MBS-QD coupling is local, and the wave functions of the MBSs at the locations where coupling happens are nearly identical. In Fig. 1, the superconducting proximity in the nanowire (purple) is supposed to be realized by epitaxy Al (see, for example, Ref. [28]) on top of it, and then the MBSs are induced at the ends of the nanowire (red points). Furthermore, the tunnel gates are covered on the tunnel junctions (purple steps) between MBSs and DQDs, and then the coupling strengths λ_1 and λ_2 could be tuned by the tunnel gates. In addition, the super gates are located at the sides of the nanowire with MBSs, and then the chemical potential in the segment covered by a superconducting shell may be tuned by the super gates. Under the resonance condition, i.e., the energy levels of DQDs are aligned to the chemical potential of the STM tip, the zero-energy spectral functions in the DQDs $A_{1(2)}(0)$ are $1/2$ regardless of the value of the relative strength of the coupling strengths V_1 and V_2,

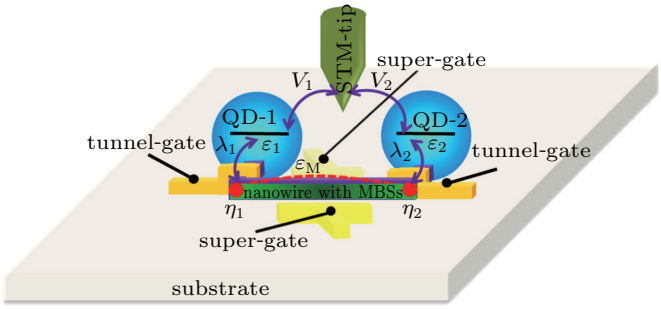


Fig. 1. Schematic plot of the hybrid STM-DQD-MBS interferometer. The system consists of a scanning tunneling STM tip (olive), DQDs (blue), and a semiconductor nanowire (purple) carrying MBSs (red) at its ends induced by a partially covered s-wave superconductor shell (green). The superconducting proximity in the nanowire (purple) is supposed to be realized by epitaxy Al[28] (green) on top of it, and then the MBSs are induced at the ends of nanowire (red points). The chemical potential in the segment covered with the superconducting shell may be tuned by applying voltages to the two long super-gates (yellow). The tunnel gates (orange steps) are employed to induce a tunnel barrier between the DQDs and the MBSs, and then tune the hybridizations λ_1 and λ_2 between the MBSs and DQDs. The coupling between MBSs η_1 and η_2 is denoted by ε_M. The energy levels of QD-1 and QD-2 are ε_1 and ε_2, respectively. The STM tip is coupled to DQDs with different coupling strengths V_1 and V_2, from which one could confirm the presence of MBSs and to probe information of MBSs. The interference contributions in the spectral functions of QDs are introduced by the electrons tunneling from QD-1 and QD-2 into the STM tip, respectively.

and the difference between the energy levels of DQDs. This indicates the formation of the MBSs in the dots. In the presence of the overlapping between the MBSs in different dots, the property of $A_{1(2)}(\omega)=1/2$ is retained in spite of the value of V_1/V_2, but it will be changed by the difference between the levels of DQDs.

The effective Hamiltonian of our model shown in Fig. 1 takes the following form:

$$H = \sum_k \varepsilon_k c_k^\dagger c_k + \sum_{j=1,2} \varepsilon_j d_j^\dagger d_j + \sum_{kj}(V_j c_k^\dagger d_j + \text{H.c.}) + H_{\text{MBS}}, \quad (1)$$

where $c_k^\dagger$ (c_k) is the creation (annihilation) operator of an electron with momentum k and energy ε_k in the STM tip, $d_j^\dagger$ (d_j, $j=1,2$) creates (annihilates) an electron in QD-j with energy level ε_j, and V_j stands for the coupling strength between QD-j and the STM tip. For simplicity, in this toy model, the Coulomb blockade in DQDs and the degree of spin freedom of electrons are ignored. The last term H_{MBS} in Eq. (1) is the effective Hamiltonian for nanowire hosting MBSs at opposite ends, which is expressed as[55,56]

$$H_{\text{MBS}} = \mathrm{i}\varepsilon_{\text{M}}\eta_1\eta_2 + \lambda_1(d_1 - d_1^\dagger)\eta_1 + \mathrm{i}\lambda_2(d_2 + d_2^\dagger)\eta_2, \quad (2)$$

where $\varepsilon_{\text{M}}\sim \mathrm{e}^{-L/\xi}$ is the coupling between the two MBSs, where L is the length of the nanowire and ξ is the superconducting coherence length. The last terms in Eq. (2) describe the coupling between MBSs and the dots with strength λ_i. The Majorana operator η_i satisfies $\eta_j=\eta_j^\dagger$ and $\{\eta_i,\eta_j\}=\delta_{ij}$. It is convenient to switch from the Majorana fermion representation to the regular fermion one by using the relationship that $\eta_1=(f^\dagger+f)/\sqrt{2}$ and $\eta_2=\mathrm{i}(f^\dagger-f)/\sqrt{2}$. The Hamiltonian H_{MBS} is then rewritten as

$$H_{\text{MBS}} = \varepsilon_{\text{M}}(f^\dagger f - \frac{1}{2}) + \frac{1}{\sqrt{2}}\sum_{i=1,2}\lambda_i(d_i - d_i^\dagger)(f^\dagger + f). \quad (3)$$

Using Green's function, we can obtain the spectral function in each QD as follows:[35]

$$A_j(\omega) = -\gamma_j \text{Im}[G^{\text{r}}_{d,jj}(\omega)], \quad (j=1,2), \quad (4)$$

where $\gamma_j = 2\pi|V_j|^2\rho_0$ is the line-width function[57,58] with $\rho_0=\sum_k \delta(\omega-\varepsilon_k)$ being the density of states in the STM tip, and $[G^{\text{r}}_{d,jj}(\omega)]$ is the retarded Green function of QD-j. The Green function can be derived by the Dyson equation

$$\boldsymbol{G}^{\text{r}}(\omega) = [\boldsymbol{g}^{\text{r}-1}(\omega) - \boldsymbol{\Sigma}^{\text{r}}]^{-1}, \quad (5)$$

where

$$\boldsymbol{g}^{\text{r}}(\omega) = \begin{bmatrix} g^{\text{r}}_{d,11} & 0 & 0 & 0 & 0 & 0 \\ 0 & \bar{g}^{\text{r}}_{d,11} & 0 & 0 & 0 & 0 \\ 0 & 0 & g^{\text{r}}_{d,22} & 0 & 0 & 0 \\ 0 & 0 & 0 & \bar{g}^{\text{r}}_{d,22} & 0 & 0 \\ 0 & 0 & 0 & 0 & g^{\text{r}}_{\text{M}} & 0 \\ 0 & 0 & 0 & 0 & 0 & \bar{g}^{\text{r}}_{\text{M}} \end{bmatrix}. \quad (6)$$

Here the electron Green function of isolated QD-1(2) is $g^{\text{r}}_{d,11(22)} = [\omega-\varepsilon_{1(2)}+\mathrm{i}0^+]^{-1}$, the hole one is $\bar{g}^{\text{r}}_{d,11(22)} = [\omega+\varepsilon_{1(2)}+\mathrm{i}0^+]^{-1}$, and the Green functions for the MBSs are written as $g^{\text{r}}_{\text{M}}=[\omega-\varepsilon_{\text{M}}+\mathrm{i}0^+]^{-1}$ and $\bar{g}^{\text{r}}_{\text{M}}=[\omega+\varepsilon_{\text{M}}+\mathrm{i}0^+]^{-1}$. The self-energy is expressed as

$$\boldsymbol{\Sigma}^{\text{r}} = \begin{bmatrix} -\frac{\mathrm{i}}{2}\gamma_1 & 0 & -\frac{\mathrm{i}}{2}\sqrt{\gamma_1\gamma_2} & 0 & \frac{\lambda_1}{\sqrt{2}} & \frac{\lambda_1}{\sqrt{2}} \\ 0 & -\frac{\mathrm{i}}{2}\gamma_1 & 0 & -\frac{\mathrm{i}}{2}\sqrt{\gamma_1\gamma_2} & -\frac{\lambda_1^*}{\sqrt{2}} & -\frac{\lambda_1^*}{\sqrt{2}} \\ -\frac{\mathrm{i}}{2}\sqrt{\gamma_1\gamma_2} & 0 & -\frac{\mathrm{i}}{2}\gamma_2 & 0 & \frac{\lambda_2}{\sqrt{2}} & -\frac{\lambda_2}{\sqrt{2}} \\ 0 & -\frac{\mathrm{i}}{2}\sqrt{\gamma_1\gamma_2} & 0 & -\frac{\mathrm{i}}{2}\gamma_2 & \frac{\lambda_2^*}{\sqrt{2}} & -\frac{\lambda_2^*}{\sqrt{2}} \\ \frac{\lambda_1^*}{\sqrt{2}} & -\frac{\lambda_1}{\sqrt{2}} & \frac{\lambda_2^*}{\sqrt{2}} & \frac{\lambda_2}{\sqrt{2}} & 0 & 0 \\ \frac{\lambda_1^*}{\sqrt{2}} & -\frac{\lambda_1}{\sqrt{2}} & -\frac{\lambda_2^*}{\sqrt{2}} & -\frac{\lambda_2}{\sqrt{2}} & 0 & 0 \end{bmatrix}. \quad (7)$$

In the STM (or say scanning tunneling spectroscopy) experiments, the tunneling current and/or the differential conductance, which is the derivative of tunneling current between the STM tip and the sample with respect to the bias, can be measured. Based on the theory of STM,[39–41] the differential conductance is proportional to the spectral functions of the QDs at the bias energy ($\omega=eV$) by $\mathrm{d}I/\mathrm{d}V \propto \sum_i A_i(\omega=eV)$. Our present work is complementary to the former studies, such as Refs. [36,53]. It is obvious that the tunneling spectroscopy of STM will provide information of the spectral functions computed theoretically. Therefore, the calculations of the spectral functions of the DQDs provide the bridge between scattering theory and the tunneling measurement of the STM. For simplicity, in the following calculations, we will concentrate on the spectral functions $A_i(\omega)$. It should be noted that the formation of the MBSs in the QD is characterized by the value of the spectral function at resonant state, i.e., $A_i(\omega=0)=1/2$. Our main goal is to examine how the spectral functions of the

DQDs are modified when the QD-MZM coupling strength λ_i, the level detuning Δ between the DQDs, and the QD-STM coupling strength $\gamma_{i=1,2}$ are changed. The STM-tip linewidth γ_1 is chosen as the energy unit and the line-width function between QD-1 and the STM tip is fixed at $\gamma_1 = 0.1$ throughout the following numerical calculations.

3. Results and discussion

Figure 2 shows the spectral functions under the conditions of $\gamma_2 = \gamma_1$, $\varepsilon_1 = \varepsilon_2 = 0$ (on-resonance) and $\varepsilon_M = 0$ for different values of λ_2. When QD-2 is decoupled from the MBSs ($\lambda_2 = 0$) as shown by the solid black lines in Fig. 2, the spectral functions at $\omega = 0$ (corresponding to the case of the energy level of QD is aligned to the Fermi energy) take a δ-type function such that $A_i(\omega) = \delta(\omega - \varepsilon_i)$ with $i = 1, 2$. There are also two broad peaks located around $\omega = \pm\lambda_1$, respectively. Now the electrons are bounded to the resonance state $\omega = \varepsilon_i$ and the information of the MBSs is overwhelmed. Turning on the coupling between QD-2 and the nanowire ($\lambda_2 = 0.03$), the spectral function $A_1(\omega)$ develops four peaks around $\omega = \pm\lambda_1, \pm\lambda_2$ due to the energy level splitting by the interaction between the QD and the MBSs as indicated by the red line in Fig. 2(a). With further increasing λ_2, the height of two peaks around $\omega = \pm\lambda_2$ is lowered, and eventually they will overlap with those around $\omega = \pm\lambda_1$. For the case of $\lambda_2 < \lambda_1$, the peaks around $\omega = \pm\lambda_1$ are almost unchanged by the value of λ_2. For $\lambda_2 \geq \lambda_1$, however, the position and height of them obviously depend on the value of λ_2. The spectral function $A_2(\omega)$ shows a double-peak configuration centered around $\omega = \pm\lambda_2$. Interestingly, the spectral function $A_{1(2)}(\omega = 0) = 1/2$ for any values of $\lambda_2 > 0$, indicating the existence of the MBSs.

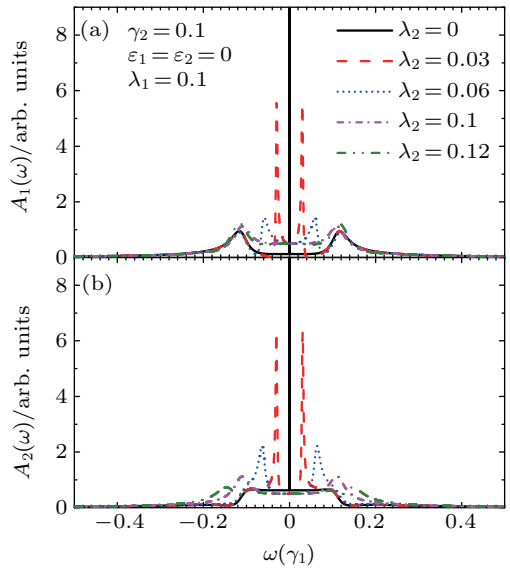


Fig. 2. Spectral functions $A_1(\omega)$ and $A_2(\omega)$ in the QD-1 and QD-2 versus the spectral frequency ω for varying the coupling strength λ_2 between QD-2 and MBSs. In the simulations, other parameters are chosen as $\gamma_1 = \lambda_1 = 0.1$, $\varepsilon_M = \varepsilon_1 = \varepsilon_2 = 0$.

In our STM-DQD-MBS model, the coupling strength between the STM tip and DQDs could be easily tuned via moving the position of the STM tip. If the STM tip is moved closer to the QD-1, then the coupling strength with QD-1 will be stronger, and the coupling strength with QD-2 will be relatively weaker. Therefore, it is necessary to study the influence of the coupling strength between the STM tip and DQDs on the spectral function. In Fig. 3 we show the impacts of the symmetry of the QD-STM coupling γ_2/γ_1 on the MBSs existing in the QD. The spectral function in QD-1 $A_1(\omega)$ shows a triple-peak configuration for $\gamma_2 = 0$ [see the black line in Fig. 3(a)]. With increasing γ_2, the two peaks around $\omega = \pm\lambda_1$ becomes more sharp and higher, and $A_1(\omega)$ changes into double-peak configuration as found in Fig. 2(a). It is found that the MBSs in QD-1 is unperturbed by the variation of γ_2, as indicated by the constant value of $A_1(0) = 1/2$. This is because the MBSs at the two ends of the nanowire are isolated for $\varepsilon_M = 0$, and the information of QD-2 cannot enter into the topologically protected zero-energy MBS in QD-1. The properties of $A_2(\omega)$ are essentially resembling to those of $A_1(\omega)$. Under the condition of $\gamma_2 = 0$, QD-2 is totally decoupled from the STM tip and the corresponding spectral function is zero [see the black line in Fig. 3(b)]. At weak γ_2, $A_2(\omega)$ shows a triple-peak configuration, which involves into a double-peak one. As long as $\gamma_2 > 0$, the spectral function at zero Fermi energy is fixed at $A_2(0) = 1/2$, indicating the stable existence of MBSs.

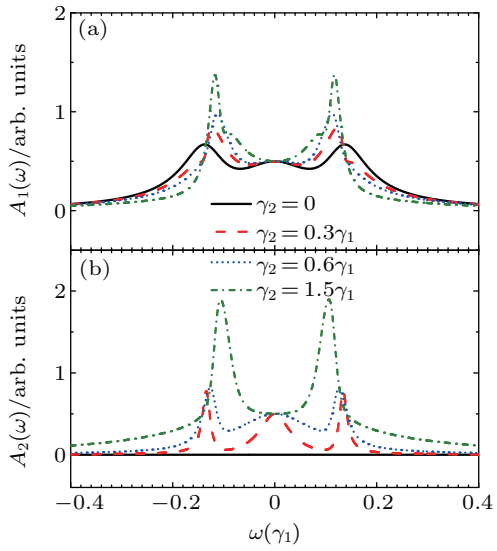


Fig. 3. Spectral functions $A_1(\omega)$ and $A_2(\omega)$ varying with ω for different values of coupling strength between the STM tip and DQ-2 γ_2. In the calculations, we choose $\lambda_2 = 0.1$, and other parameters are the same as those in Fig. 2.

The energy levels of DQDs are respectively considered as ε_1 and ε_2 in our model. In the above calculations of Figs. 2 and 3, $\varepsilon_1 = \varepsilon_2 = 0$ is chosen. In fact, the energy levels of DQDs may be different from each other, which could be easily tuned in experiments. Therefore, it is necessary to analyze influence of the difference between the energy levels of DQDs on the

effective tunneling of the MBSs into the QD. Here, the difference between the energy levels of DQDs, i.e., levels' detuning Δ is defined as $\varepsilon_{1(2)} = \varepsilon_0 + (-)\Delta/2$. Typical results of spectrum function $A_i(\omega)$ for several values of levels' detuning Δ are shown in Fig. 4. For the case of $\lambda_1 = 0.1$ and $\lambda_2 = 0.06$ as shown in Fig. 4(a), $A_1(\omega)$ (thick lines) has four peaks under the condition of $\Delta = 0$, which are symmetric with respective to the point of $\omega = 0$, as found in Fig. 2(a). In the presence of the levels' detuning, namely $\Delta \neq 0$, the peaks move toward lower energy regime with the reduction of the hight of peaks. The value of $A_1(0)$, however, remains unchanged and the MBS bounded to QD-1 is quite stable against the level difference between the QD. Similar to the behavior of $A_1(\omega)$, the peaks in $A_2(\omega)$ (thin lines) move toward high energy region while the height of peaks are suppressed and the zero energy spectral function remains a half of unity, i.e., $A_2(0) = 1/2$. If $\lambda_1 = \lambda_2$ as shown in Fig. 4(b), $A_1(\omega)$ (thick lines) and $A_2(\omega)$ (thin lines) are mirror symmetric to $\omega = 0$, and the characters of the peaks resemble those of in Fig. 4(a). As a consequence, Fig. 4 demonstrates that the topologically protected Majorana zero-energy mode in our STM-DQD-MBS interferemeter are insensitive to the variation of the energy levels of DQDs since electrons can hardly enter into these states. Moreover, we find that these MBSs formed in the DQDs are stable regardless of the relative strengths of λ_1 and λ_2.

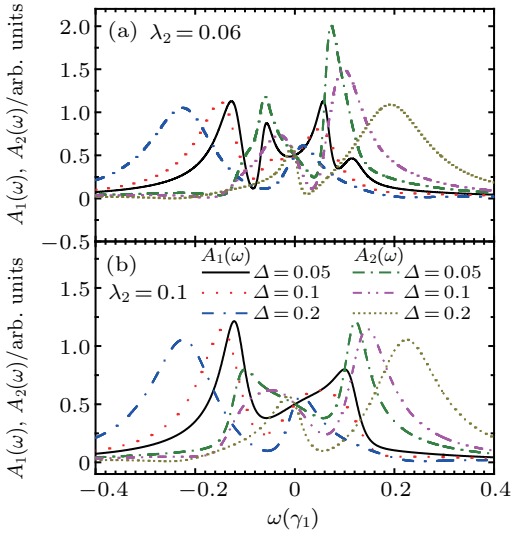


Fig. 4. Spectral functions $A_1(\omega)$ (thick lines) and $A_2(\omega)$ (thin lines) versus ω for different levels detuning Δ between QD-1 and QD-2. In the calculations, $\lambda_2 = 0.06$ for (a) and $\lambda_2 = 0.1$ for (b) are chosen, and other parameters are the same as those in Fig. 2.

In all the above discussions, the overlap between the two MBSs is not considered ($\varepsilon_M = 0$), while in Fig. 5 we present the spectral functions in the presence of overlap between the two MBSs ($\varepsilon_M \neq 0$). First of all, we find that the zero energy spectral functions remain numerically unchanged, i.e., $A_{1(2)}(0) = 1/2$, regardless of the value of ε_M in both the asymmetric hybridization case of $\lambda_1 > \lambda_2$ [see Figs. 5(a) and 5(b)] and the symmetric hybridization case of $\lambda_1 = \lambda_2$ [see Fig. 5(c)]. For the general cases with various parameters, such as ε_1, ε_2, λ_1, λ_2, γ_1, γ_2, and ε_M shown in our model, it is difficult to get a compactly analytical expression of Green's function of QDs in the presence of MBSs. However, for a special case of $\gamma_1 = \gamma_2 = \gamma$, $\lambda_1 = \lambda_2 = \lambda$, and $\varepsilon_1 = \varepsilon_2 = 0$, a compact expression of zero-energy Green's function of QD $G_{d,i}(\omega \to 0)$ may be approximated as

$$G_{d,i}(\omega \to 0) \approx \frac{\varepsilon_M - i\omega^+}{\lambda^2 + i\omega^+} - i\frac{\lambda^2}{\gamma\lambda^2 - i\omega^+} - i\frac{\lambda^4}{\gamma\lambda^4 + i\omega^+}, \tag{8}$$

where $i\omega^+ = \omega + i0^+$. In the limit of $\omega \to 0$, the imaginary part of $G_{d,i}(\omega \to 0)$ may be written as $\mathrm{Im}\left[G_{d,i}(\omega \to 0)\right] \approx -\frac{1}{2\gamma}$, which just depends on the STM-QD coupling strength, but does not depend on the overlap between the two MBSs ε_M. Substituting this formula into Eq. (4), one could easily get $A_i(\omega \to 0) = \frac{1}{2}$, which is consistent with our numerical results shown in Fig. 5. This result indicates that the MZM could be stored in the QDs even in the presence of the overlap between the two MBSs ε_M.[19,35,55] Secondly, the height and positions of the peaks of $A_i(\omega)$ are sensitive to the value of ε_M with retained peak configuration. For instance, we could observe from Fig. 5(a) that the peaks around $\omega = \pm\lambda_1(\pm\lambda_2)$ are shifted away from (toward) the zero energy point by increasing ε_M with the reduction of them. Simultaneously, the height of $A_1(\omega)$ originally around $\omega = \pm\lambda_1$ is suppressed with increasing ε_M. Moreover, the peak originally around $\omega = -\lambda_2$ will evolve into a dip as shown in Fig. 5(a), and the peak around $\omega = \lambda_2$ is narrowed and enhanced. The evolution of the double peaks in $A_2(\omega)$ resemble those of $A_1(\omega)$ around $\omega = \pm\lambda_2$, see Fig. 5(b). For the symmetric hybridization case of $\lambda_1 = \lambda_2$, the spectral functions of the DQDs are equal to each other. With the increase of ε_M, we find that the double peaks of $A_{i=1,2}(\omega)$ in the positive and negative energy regimes are shifted toward and away from the zero energy point, respectively. Meanwhile, the peak height in the positive (negative) energy regime is enhanced (lowered). Moreover, a dip at negative energy regime emerges due to the quantum interference effect.

In Figs. 6(a) and 6(b) we show the impact of different values of γ_2 on the spectral functions with a fixed overlap between MBSs. For instance, in Figs. 6(a) and 6(b) $\varepsilon_M = 0.02$ is chosen. Differing from Fig. 3 for the case of $\varepsilon_M = 0$, we can clearly find from Figs. 6(a) and 6(b) that the symmetry of the spectral functions is broken due to the nonzero overlap between MBSs. From Fig. 6(a), we observe that the four-peak configuration of $A_1(\omega)$ evolves a triple-peak one with increasing γ_2. This is because the interference effect between the DQDs via the STM tip becomes stronger. The peak around $\omega = -\lambda_2$ is emerged into that of $\omega = \lambda_2$, leading to the higher

peak. With increasing γ_2, $A_2(\omega)$ develops a triple peaks whose positions are almost unchanged by the value of γ_2, whereas they become higher with increasing λ_2, see Fig. 6(b). It is a natural result that $A_2(\omega) = 0$ when the coupling between the STM tip and QD-2 is absent ($\gamma_2 = 0$), see the black line in Fig. 6(b). It is not surprising that we find $A_i(0) = 1/2$ for any nonzero coupling strength $\gamma_{i=1,2}$, which is consistent with the above discussions. Finally, in Fig. 6(c) we give the results of zero energy spectral functions $A_1(\omega = 0)$ and $A_2(\omega = 0)$ varying with energy level detuning Δ between DQDs for different overlap of MBSs ε_M. For the case of $\varepsilon_M = 0$, both $A_1(\omega)$ and $A_2(\omega)$ are equal to $1/2$ regardless of the value of Δ. For the case of $\varepsilon_M \neq 0$, the spectral functions of DQDs equal to $1/2$ only for $\Delta = 0$, and are mirror-symmetric with respective to $\Delta = 0$. They also develop peaks for nonzero ε_M.

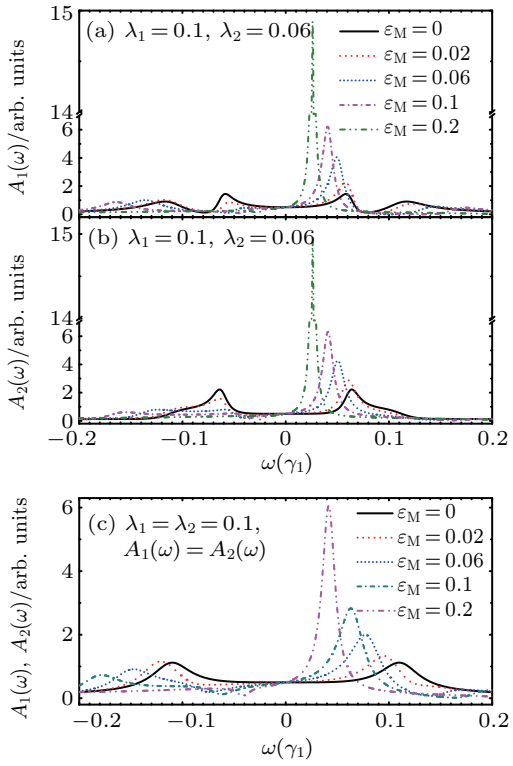


Fig. 5. Spectral functions varying with ω for different values of the coupling between the two MBSs ε_M. In the calculations, the hybridization between MBSs and QD-2 is chosen as $\lambda_2 = 0.06$ in (a) and (b), and $\lambda_2 = 0.1$ in (c). Other parameters are the same as those in Fig. 2.

In all calculations of Figs. 2–6, we assume that the nanowire is driven into the topological phase that the MBSs exit at the ends of the nanowire. The MBSs at the end of the nanowire significantly influence the spectrum function of QD. A significant feature is that when MBSs and QDs are coupled with each other, no matter how other tunable parameters (such as coupling strength between the STM tip and QD, energy level detuning between QD-1 and QD-2, coupling between the two MBSs, and others) change within a reasonable range, the zero energy spectrum function of the QD always remains $A_i(0) = 1/2$. When MBSs and QDs are decoupled with each other, i.e., $\lambda_1 = \lambda_2 = 0$, the zero energy spectrum function of QD will be tuned by the coupling strength between the STM tip and the QD, the energy level detuning between QD-1 and QD-2, and other parameters. Especially, for the trivial case that $\lambda_1 = \lambda_2 = 0$, $\varepsilon_1 = \varepsilon_2 = 0$, and $\gamma_1 = \gamma_2 = \gamma$, the spectrum function of QD-i may be written as $A_i(\omega) = \frac{1}{\pi}\frac{\gamma/2}{\omega^2+\gamma^2}$, and then $A_i(\omega = 0) = \frac{1}{2\pi\gamma}$. It is clear that a sharp jump in the zero energy spectrum function of QD by a factor of $1/2$ is universal as long as the MBSs are taken into account and couple to the QD.[36,37,55] Therefore, the spectrum function of QD, especially the zero energy spectrum function of QD, may be an evidence of the presence of MBSs, and then our model may provide a potential way to prob the MBSs.

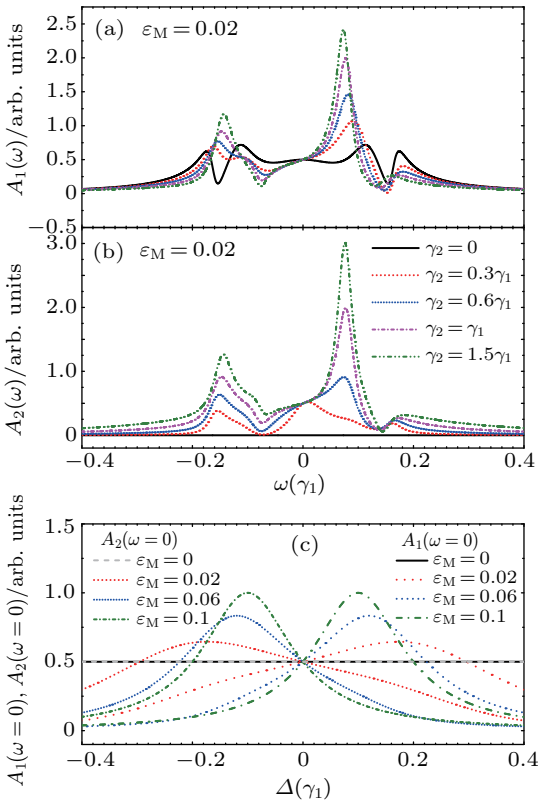


Fig. 6. (a) and (b) Spectral functions $A_1(\omega)$ and $A_2(\omega)$ varying with ω for different values of coupling strength between the STM tip and QD-2 γ_2. (c) $A_1(\omega)$ and $A_2(\omega)$ as functions of levels detuning Δ for different overlap between MBSs ε_M. In all the calculations, symmetric coupling between STM and DQDs is considered by $\lambda_1 = \lambda_2 = 0.1$. In (a) and (b), the overlap between MBSs is chosen as $\varepsilon_M = 0.06$. Other parameters are the same as those in Fig. 2.

Furthermore, our model could be easily generalized to a spin-polarized one. In other words, the STM tip could be assumed as an spin-polarized one. By applying an external magnetic field, the spin degeneceracy of energy levels of QD may be split via the Zeeman effect, and the spin of MBSs will be also polarized to a fixed direction (spin-up or spin-down). Thereby, the spin dependent tunneling effect and the spin blocked effect could be naturally taken into account in the spin-polarized model. As a result, the spin-resolved spectral function may be easily detected via a spin-polarized STM-

DQD-MBS system, and the spin dependent effects therein may provide more interesting information and more direct evidence of Majorana zero modes in condensed matter. We will thoroughly study the spin polarized model in another work since it is beyond the scope of this work.

4. Conclusion

We have investigated the properties of the spectral functions in a DQD system coupled to a normal metallic STM tip and MBSs in a semiconductor-superconductor nanowires. It is found that the zero-energy spectral functions are always equal to half of unity, which indicates the formation of the MBSs in the QD and the zero-bias conductance peak. If the MBSs in DQDs are overlapped, the formation of the MBSs is favorable for the case of identical levels of QD. The presently advanced STM technology and quantum device fabrication technology enable our theoretical model to be easily implemented in experiments to validate our theoretical results. Therefore, we hope our theoretical findings in this work could be experimentally checked in the near future.

References

[1] Hasan M Z and Kane C L 2010 *Rev. Mod. Phys.* **82** 3045
[2] Qi X L and Zhang S C 2011 *Rev. Mod. Phys.* **83** 1057
[3] Kitaev A Y 2001 *Phys. Usp.* **44** 131
[4] Fu L and Kane C 2008 *Phys. Rev. Lett.* **100** 096407
[5] Alicea J 2012 *Rep. Prog. Phys.* **75** 076501
[6] Klinovaja J and Loss D 2012 *Phys. Rev. B* **86** 085408
[7] Yin J X, Wu Z, Wang J H *et al.* 2015 *Nat. Phys.* **11** 543
[8] Hu H, Zhang F and Zhang C 2018 *Phys. Rev. Lett.* **121** 185302
[9] Hsu C H, Stano P, Klinovaja J and Loss D 2018 *Phys. Rev. Lett.* **121** 196801
[10] Nayak C, Simon S H, Stern A, Freedman M and Das Sarma S 2008 *Rev. Mod. Phys.* **80** 1083
[11] Zhou Y F, Hou Z and Sun Q F 2019 *Phys. Rev. B* **99** 195137
[12] Lutchyn R, Sau J D and Das Sarma S 2010 *Phys. Rev. Lett.* **105** 077001
[13] Oreg Y, Refael G and von Oppen F 2010 *Phys. Rev. Lett.* **105** 177002
[14] Albrecht S M, Higginbotham A P, Madsen M, Kuemmeth F, Jespersen T S, Nygård, Krogstrup P and Marcus C M 2016 *Nature* **531** 206
[15] Deng M T, Vaitiek_enas S, Hansen E B, Danon J, Leijnse M, Flensberg K, Nygård J, Krogstrup P and Marcus C M 2016 *Science* **354** 1557
[16] Deng M T, Vaitieküenas S, Prada E, San-Jose P, Nygård J, Krogstrup P, Aguado R and Marcus C M 2018 *Phys. Rev. B* **98** 085125
[17] Hays M, de Lange G, Serniak K, van Woerkom D J, Bouman D, Krogstrup P, Nygård J, Geresdi A and Devoret M H 2018 *Phys. Rev. Lett.* **121** 047001
[18] Lutchyn R M, Bakkers E P A M, Kouwenhoven L P, Krogstrup P, Marcus C M and Oreg Y 2018 *Nat. Rev. Mater.* **3** 52
[19] Shang E C, Pan Y M, Shao L B and Wang B G 2014 *Chin. Phys. B* **23** 057201
[20] Jiang Z T and Zhong C C 2016 *Chin. Phys. B* **25** 067302
[21] Moore C, Stanescu T D and Tewari S 2018 *Phys. Rev. B* **97** 165302
[22] Li J, Yu T, Lin H Q and You J Q 2015 *Sci. Rep.* **4** 4930
[23] Rubbert S and Akhmerov A R 2016 *Phys. Rev. B* **94** 115430
[24] Hell M, Flensberg K and Leijnse M 2018 *Phys. Rev. B* **97** 161401(R)
[25] Schuray A, Weithofer L and Recher P 2017 *Phys. Rev. B* **96** 085417
[26] Liu C X, Sau J D, Stanescu T D and Das Sarma S 2017 *Phys. Rev. B* **96** 075161
[27] Li Y, Li S X, Lidag H O, Deng G W, Cao G, Xiao M and Guo G P 2018 *Chin. Phys. B* **27** 76105
[28] Zhang H *et al.* 2018 *Nature* **556** 74
[29] Li X Q and Xu L 2020 *Phys. Rev. B* **101** 205401
[30] Zhu S, Kong L, Cao L *et al.* 2020 *Science* **367** 189
[31] Liu C X, Cole W S and Sau J D 2019 *Phys. Rev. Lett.* **122** 117001
[32] Feng J J, Huang Z, Wang Z and Niu Q 2018 *Phys. Rev. B* **98** 134515
[33] Virtanen P, Bergeret F S, Strambini E, Giazotto F and Braggio A 2018 *Phys. Rev. B* **98** 020501(R)
[34] Liu D T, Shabani J and Mitra A 2019 *Phys. Rev. B* **99** 094303
[35] Ricco L S, de Souza M, Figueira M S, Shelykh I A and Seridonio A C 2019 *Phys. Rev. B* **99** 155159
[36] Cifuentes J D and da Silva L G G V 2019 *Phys. Rev. B* **100** 085429
[37] Wang N, Lv S H and Li Y X 2014 *J. Appl. Phys.* **115** 083706
[38] Ramos-Andrade J P, Orellana P A and Vernek E 2020 *Phys. Rev. B* **101** 115403
[39] Binnig G, Rohrer H, Gerber C *et al.* 1982 *Phys. Rev. Lett.* **49** 57
[40] Binnig G and Rohrer H 1987 *Rev. Mod. Phys.* **59** 615
[41] Balatsky A V, Vekhter I and Zhu J X 2006 *Rev. Mod. Phys.* **78** 373
[42] You S F *et al.* 2019 *Acta Phys. Sin.* **68** 016802 (in Chinese)
[43] Sun H H *et al.* 2016 *Phys. Rev. Lett.* **116** 257003
[44] Jeon S, Xie Y, Li J, Wang Z, Bernevig B A and Yazdani A 2017 *Science* **358** 772
[45] Wang D, Kong L, Fan P *et al.* 2018 *Science* **362** 333
[46] Machida T, Sun Y, Pyon S, Takeda S, Kohsaka Y, Hanaguri T, Sasagawa T and Tamegai T 2019 *Nat. Mater.* **18** 811
[47] Kong L, Zhu S, Papaj M *et al.* 2019 *Nat. Phys.* **15** 1181
[48] Jäck B, Xie Y, Li, J, Jeon S, Bernevig B A and Yazdani A 2019 *Science* **364** 1255
[49] Chen C, Jiang K, Zhang Y, Liu C, Liu Y, Wang Z and Wang J 2020 *Nat. Phys.* **16** 536
[50] Pan Y, Yang J, Erwin S C, Kanisawa K and Fölsch S 2015 *Phys. Rev. Lett.* **115** 076803
[51] Chevallier D and Klinovaja J 2016 *Phys. Rev. B* **94** 035417
[52] Devillard P, Chevallier D and Albert M 2017 *Phys. Rev. B* **96** 115413
[53] Górski G, Barański J, Weymann I and Domański T 2018 *Sci. Rep.* **8** 15717
[54] Wang J 2018 *Phys. Rev. B* **98** 024519
[55] Liu D E and Baranger H U 2011 *Phys. Rev. B* **84** 201308(R)
[56] Ricco L S, Campo Jr. V L, Shelykh I A and Seridonio A C 2018 *Phys. Rev. B* **98** 075142
[57] Sun Q F, Xing Y X and Shen S Q 2008 *Phys. Rev. B* **77** 195313
[58] Liu J, Sun Q F and Xie X C 2010 *Phys. Rev. B* **81** 245323